# Charge transfer and hybridization effects in $Ni_3Al$ and $Ni_3Ga$ studies by x-ray-absorption spectroscopy and theoretical calculations

Y. K. Chang, K. P. Lin, and W. F. Pong[a)]
*Department of Physics, Tamkang University, Tamsui 251, Taiwan*

M.-H. Tsai
*Department of Physics, National Sun Yat-Sen University, Kaohsiung 804, Taiwan*

H. H. Hseih, J. Y. Pieh,[b)] and P. K. Tseng
*Department of Physics, Tamkang University, Tamsui 251, Taiwan*

J. F. Lee
*Synchrotron Radiation Research Center, Hsinchu Science-based Industrial Park 300, Taiwan*

L. S. Hsu
*Department of Physics, National Chang-Hua University of Education, Chang-Hua 500, Taiwan*

(Received 10 May 1999; accepted for publication 21 October 1999)

This work investigates the charge transfer and Al(Ga) *p*-Ni *d* hybridization effects in the intermetallic $Ni_3Al$ ($Ni_3Ga$) alloy using the Ni $L_{3,2}$ and *K* edge and Al (Ga) *K* x-ray absorption near edge structure (XANES) measurements. We find that the intensity of near-edge features at the Ni $L_3$ edge in the $Ni_3Al$ ($Ni_3Ga$) alloy decreased with respect to that of pure Ni, which implies a reduction of the number of unoccupied Ni $3d$ states and an enhancement of the Ni $3d$ state filling in the $Ni_3Al$ ($Ni_3Ga$) alloy. Two clear features are also observed in the $Ni_3Al$ ($Ni_3Ga$) XANES spectrum at the Al (Ga) *K* edge, which can be assigned to unoccupied Al $3p$-(Ga $4p$-) derived states in $Ni_3Al$ ($Ni_3Ga$). The threshold at the Al *K*-edge XANES for $Ni_3Al$ shifts towards the higher photon energy relative to that of pure Al, suggesting that Al loses some *p*-orbital charge upon forming $Ni_3Al$. On the other hand, the Ni *K* edge shifts towards the lower photon energy in $Ni_3Al$ ($Ni_3Ga$) relative to that of pure Ni, suggesting a gain of charge at the Ni site. Thus both Al and Ni *K*-edge XANES results imply a transfer of charge from Al $3p$ orbital to Ni sites. Our theoretical calculations using the spin-polarized first-principles pseudofunction method agree with these results. © *2000 American Institute of Physics.* [S0021-8979(00)03603-3]

## I. INTRODUCTION

The intermetallic $Ni_3Al$ compound has received extensive attention owing to its potential applications in high-temperature structural materials.[1] The unique properties of the $Ni_3Al$ compound are principally attributed to the nature of its electronic and atomic structures. It is well known that the atomic structure of $Ni_3Al$ has a cubic $LI_2$-type order. In this structure Al occupies the cubic corners and Ni occupies the face centers so that each Ni atom is coordinated with 8 Ni and 4 Al atoms in the first shell. Extended electron energy-loss fine structure studies were performed on the local atomic structure of $Ni_3Al$.[2] On the other hand, Muller *et al.*[3] performed Ni $L_{3,2}$-edge electron energy loss spectroscopy (EELS) to investigate the electronic structure of segregated grain boundaries in $Ni_3Al$ with and without boron dopants. This study indicated that boron tends to increase the cohesive strength, possibly due to the enhancement of boron-induced ductility in $Ni_3Al$. Owing to the absence of a core level shift in the Ni $L_3$-edge EELS spectra of $Ni_3Al$ from that of pure Ni, Muller *et al.* concluded that little net charge is transferred between Al and Ni sites in $Ni_3Al$. And Auger electron[4] and x-ray photoemission[5] measurements suggested that charge transfer only influences slightly the filling of the Ni $3d$ band in $Ni_3Al$. Iotova *et al.* systematically calculated electronic structures and elastic properties for the $Ni_3X$ (X=Mn, Al, Ga, Ge, and Si) series and found an increasing trend of shear module that goes from $Ni_3Mn$ to $Ni_3Si$.[6] This trend could be related to the anisotropic bonding charge density resulted from a combination of the charge transfer from X to Ni and a strong X $p$-Ni $d$ (Mn $d$-Ni $d$ in $Ni_3Mn$) hybridization effects in $Ni_3X$. Charge transfer and strong hybridization effects in $Ni_3Al$ were also supported by previous electronic structure calculations.[7,8] Thus, there were discrepancies between theoretical results and the interpretations of EELS, Auger, and x-ray photoemission data. As generally known, the charge transfer between X and Ni sites and the density of X $p$-Ni $d$ hybridized states above the Fermi level in the $Ni_3X$ systems should be observable for all excitations involving outermost X $p$ or Ni $d$ final states from x-ray absorption near edge structure (XANES) spectra. Here, we focus on the understanding of the *p-d* hybridization between Al and Ni in $Ni_3Al$ and between Ga and Ni in $Ni_3Ga$ and clarification of the controversy over the charge transfer between Al (Ga) and Ni sites in $Ni_3Al$ ($Ni_3Ga$). How charge transfer influences the filling of the Ni $3d$ band in $Ni_3Al$ ($Ni_3Ga$) will be addressed.

a)Electronic mail: wfpong@mail.tku.edu.tw
b)Author to whom correspondence should be addressed; present address: China Textile Institute, Tu-Chen, Taiwan.

 

TABLE I. The parameters of the lattice constant ($a_0$), muffin-tin radii ($R_{mt}$), and number of plane waves which we used to expand the psuedofunction (PSF), charge density $\rho$, and potential $V$ at the interstitial and nonspherical regions.

| | $a_0$(a.u.) | $R_{mt(a.u.)}$ | PSFs | $\rho$ | $V$ |
|---|---|---|---|---|---|
| Ni | 6.6519[a] | 2.17 | $13^3$ | $25^3$ | $25^3$ |
| $Ni_3Al$ | 6.7378 | 2.35 (Ni)<br>2.38 (Al) | $9^3$ | $17^3$ | $17^3$ |
| $Ni_3Ga$ | 6.7841 | 2.35 (Ni)<br>2.44 (Ga) | $9^3$ | $17^3$ | $17^3$ |
| Al | 7.6535[a] | 2.30 | $11^3$ | $21^3$ | $21^3$ |

[a]C. Kittel, *Introduction to Solid State Physics*, 7th ed. (J Wiley, New York, 1996).

The chemical shifts of the absorption edge in the XANES spectra are strongly related to the charge transfer between Al (Ga) and Ni sites. We also analyzes the electronic structures of $Ni_3Al$ ($Ni_3Ga$) obtained by combining Ni $L_{3,2}$- and $K$ edge and Al (Ga) $K$-edge XANES measurements and the spin-polarized first-principles electronic structure calculations using the pseudofunction method.

## II. EXPERIMENT

The XANES measurements were performed using the high-energy spherical grating monochromator (HSGM) with an electron beam energy of 1.5 GeV and a maximum stored current of 200 mA at the Synchrotron Radiation Research Center (SRRC), Hsinchu, Taiwan. The spectra of the Ni $L_{3,2}$ edge and Al $K$-edge XANES were measured using the sample drain current mode at the room temperature. The Ni and Ga $K$-edge XANES measurements were also performed in a total electron mode at the wiggler beamline of SRRC. A Si(111) double crystal monochromator was used to record the spectra. The typical resolution of the spectra was 0.4–0.5 eV for HSGM and ~2 eV for wiggler beamlines. The samples were prepared by arc melting after argon backfill, as described in elsewhere.[9] The single phase and concentration of the samples were confirmed using x-ray diffraction and energy-dispersive x-ray fluorescence analysis.

## III. THEORY

The spin-polarized first-principles pseudofunction (PSF) method[10] was employed to calculate the projected density-of-states (DOS) and the amount of electron charge occupying each valence state at the Ni and Al sites in the $Ni_3Al$ and $Ni_3Ga$ alloys and pure Ni and Al reference samples. In this method, the potential was divided into spherical potentials within the muffin-tin spheres and a plane-wave expanded potential that extends throughout the crystal, which includes interstitial potential and the nonspherical part of potentials within muffin-tin spheres. PSFs are smooth mathematical functions constructed by continuously and differentially extending the muffin-tin-orbital tails into muffin-tin spheres. They are simply devised to calculate the interstitial and nonspherical parts of matrix elements efficiently[10] through plane waves using the fast Fourier transform technique. Table I lists the lattice constant ($a_0$), muffin-tin radii ($R_{mt}$), and number of plane waves used to expand the PSF, nonspherical and interstitial charge density $\rho$ and potential $V$ for all the samples. The lattice constants of $Ni_3Al$ and $Ni_3Ga$ were determined according to the x-ray diffraction measurements. The unit-cell parameters and atomic positions were deduced from x-ray crystallograph table.[11] Muffin-tin radii chosen for Ni, Al, and Ga are roughly proportional to their covalent radii[12] with the constraint that all muffin-tin spheres do not overlap. We have chosen the cubic unit cell for $Ni_3Al$, $Ni_3Ga$, and pure Ni and Al metals, although they have a face-centered-cubic (fcc) base structure. For pure Ni and Al, there are four Ni or Al atoms per unit cell. For $Ni_3Al$ and $Ni_3Ga$, there are three Ni atoms and one Al or Ga atom in the unit cell. In this study, four special **k** points of Chadi and Cohen for a simple cubic lattice were used to obtain the self-consistent charge density and potential.[13] To obtain partial DOSs, we have chosen the Monkhorst–Pack special **k** points with $\mathbf{q}=4$.[14] Totally, twenty special **k** points were sampled to obtain partial DOSs.

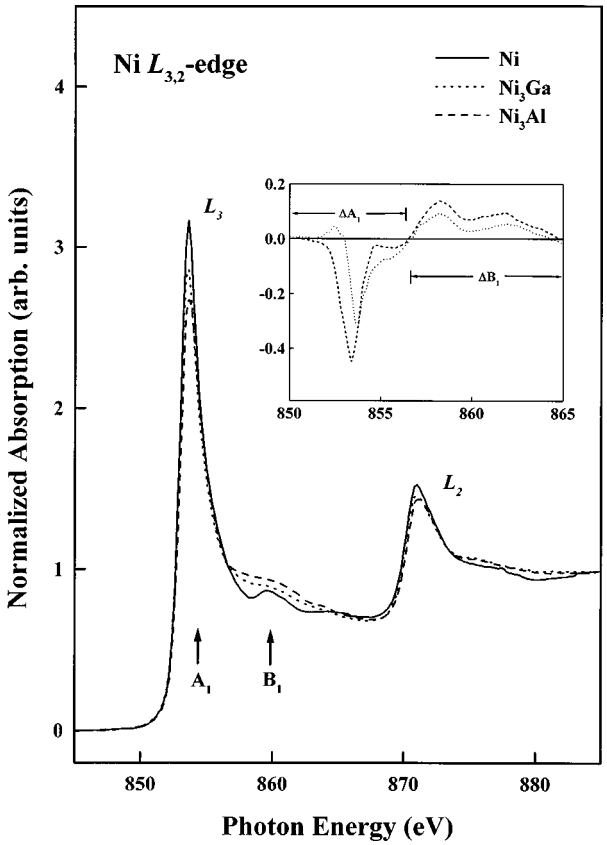


FIG. 1. Normalized Ni $L_{3,2}$-edge x-ray absorption spectra of $Ni_3Al$ and $Ni_3Ga$ alloys and pure Ni metal at room temperature. The inset shows the Ni $L_3$-edge difference curve for $Ni_3Al$ and $Ni_3Ga$ with respect to pure Ni.

## IV. RESULTS AND DISCUSSION

Figures 1 and 2 display the Ni $L_{3,2}$ and Al $K$-edge XANES spectra of the $Ni_3Al$ and $Ni_3Ga$ alloys, respectively, in which pure Ni and Al metals are regarded as references. All of the spectra shown in these figures were divided by the incident intensity $I_0$ and then normalized to an edge jump of unity. The normalization procedure was implemented by matching the absorption coefficients from the pre-edge re-

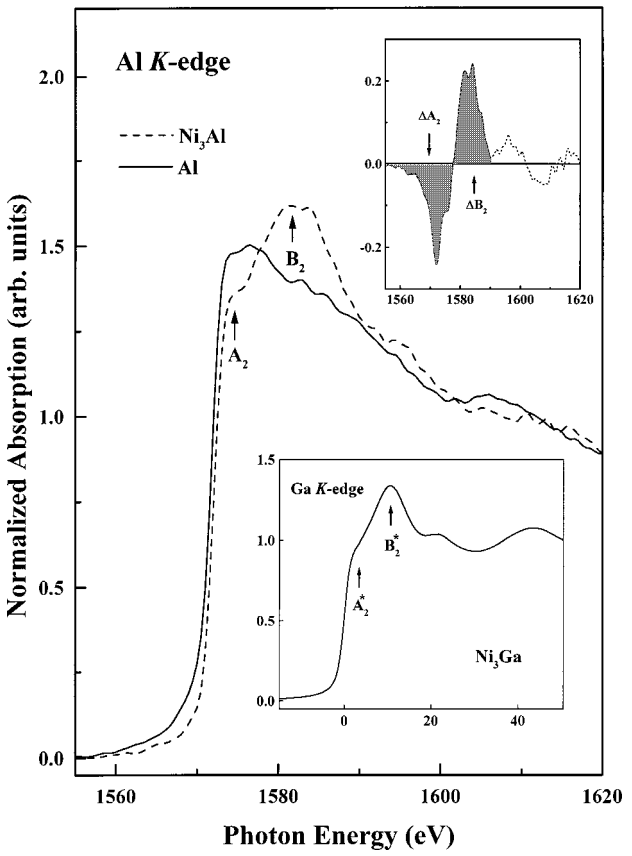


FIG. 2. Normalized Al *K*-edge x-ray absorption spectra of $Ni_3Al$ (dot line) and pure Al (solid line) at room temperature. The lower inset shows the normalized Ga *K*-edge x-ray absorption spectra of the $Ni_3Ga$ alloy, in which the zero energy was selected at the reflection point of the edge. The upper inset shows the Al *K*-edge difference curve between $Ni_3Al$ and Al. The area under the difference curve in the region of interest is darkened.

gion at $L_3$ edge to 20 eV above the $L_2$ edge of Ni and keep the same area in the energy range between 1660 and 1670 eV (not fully shown in Fig. 2) as that of the Al *K* edge. By using the dipole-transition selection rules, we can assign the white line features at the Ni $L_{3,2}$-edge (labeled $L_3$ and $L_2$) XANES to the transitions from the Ni $2p_{3/2}$ and $2p_{1/2}$ ground states to the unoccupied Ni $3d$ final states. The general spectral lineshapes in the Ni $L_{3,2}$-edge XANES spectra of $Ni_3Al$ and $Ni_3Ga$ display similar white-line features (labeled as $A_1$) above the Ni $L_3$ edge. However, their intensities are reduced considerably in comparison with those of pure Ni. The dependence of the general behavior of the spectra's line shape and intensity on the photon energy for $Ni_3Al$ and $Ni_3Ga$ are similar except that the intensity of the white-line features $A_1$ (the higher energy satellite structure, $B_1$) at the Ni $L_3$ edge is slightly lower (larger) in the $Ni_3Al$ spectrum than in the $Ni_3Ga$ spectrum. The difference curve (hereinafter referred to as $\Delta A_1$ and $\Delta B_1$) of the Ni $L_3$-edge XANES in $Ni_3Al$ and $Ni_3Ga$ with respect to pure Ni are shown in the inset of Fig. 1. No significant energy shifts of the highest peak in the Ni $L_{3,2}$-edge XANES spectra from that of pure Ni are observed for both alloys. Our data are in agreement with earlier Ni $L_{3,2}$-edge EELS measurements made on the $Ni_{1-x}Al_x$ alloys.[3] In addition, the satellite structures $B_1$ for both $Ni_3Al$ and $Ni_3Ga$ are enhanced and broadened relative to that of pure Ni. This satellite structure can be assigned to the excitation of electrons from Ni $2p_{3/2}$ to Ni $4s$ states.[15] Our results indicate a decrease in the intensity of white-line features $A_1$ at the Ni $L_3$ edge for both $Ni_3Al$ and $Ni_3Ga$ alloys relative to that of pure Ni, which corresponds to a decrease of the number of unoccupied Ni $3d$ states and an enhancement of the Ni $3d$-state filling.

Figure 2 displays the Al *K*-edge XANES spectra for $Ni_3Al$ and pure Al. In the $Ni_3Al$ spectrum, the intensity of feature $A_2$, which is located between ~1573 and 1577 eV, is markedly reduced and the reflection point of the threshold clearly shifts towards the higher energy with respect to that of pure Al. In addition, a prominent feature $B_2$ (located between ~1577 and 1590 eV) is significantly enhanced in the $Ni_3Al$ spectrum. The lower inset of this same figure reveals a similar behavior of features $A_2^*$ and $B_2^*$ at the Ga *K*-edge XANES in the $Ni_3Ga$ spectrum (There was a difficulty in comparing the Ga *K*-edge XANES spectrum with that of pure Ga because pure Ga has a low melting point and different bonding properties at room temperature). According to the dipole-transition selection rules, the features $A_2$ ($A_2^*$) and $B_2$ ($B_2^*$) in the Al (Ga) *K*-edge XANES spectra as shown in the (inset) of Fig. 2 can be assigned to the transitions to unoccupied Al $3p$-(Ga $4p$-) derived states, which hybridize with the Ni $3d/4sp$ states. As mentioned earlier, the inflection point in the $Ni_3Al$ XANES spectrum at the Al *K* edge apparently shifts towards the higher photon energy than those of pure Al. This suggests that Al loses some *p*-orbital charge upon forming $Ni_3Al$ because the loss of some $3p$ electrons reduces the screening of the Al nuclear charge and consequently lowers the $1s$ core level energy of Al. We also determine the difference of the densities of Al $3p$-derived states for $Ni_3Al$ and pure Al just above the Fermi level. A comparison is made of the areas under the Al *K*-edge XANES spectra as shown in Fig. 2. The edge energy $E_0$ in the $Ni_3Al$ spectra is aligned with that of pure Al. We assume that the dipole transition matrix element at the Al *K* edge is the same for both $Ni_3Al$ and pure Al. We also adopt the findings of Tamura *et al.* for pure Al that its unoccupied *p* states spread up to ~30 eV above the Fermi level[16] and that the area under the difference curve (hereinafter denoted as $\Delta A_2$ and $\Delta B_2$) as shown in the upper inset of Fig. 2 is proportional to the difference in the densities of unoccupied Al $3p$-derived states between $Ni_3Al$ and pure Al. The ranges of integration are from 1555.0 to 1577.5 eV and from 1577.5 to 1590.0 eV, respectively, for $\Delta A_2$ and $\Delta B_2$. The integration for $\Delta A_2 + \Delta B_2$ yields 0.17 ($-1.56 \pm 0.08$ and $1.73 \pm 0.09$, respectively, for $\Delta A_2$ and $\Delta B_2$). Thus, the number of unoccupied Al $3p$-derived states increases in $Ni_3Al$ relative to that of pure Al. In other words, Al loses some *p*-orbital charge in consistent with that suggested by the shift of the threshold of the spectrum.

Ni $L_{3,2}$- and Al *K*-edge XANES results suggest a charge transfer from the Al $3p$ orbitals to Ni sites. However, in metals the charge count at the atomic site (Wigner Seitz volume) tends to remain neutral, i.e., only a small amount of net charge transfer possibly occurs upon alloying. This property is due to the itinerant nature of conduction electrons which automatically adjust their distribution to minimize the elec-

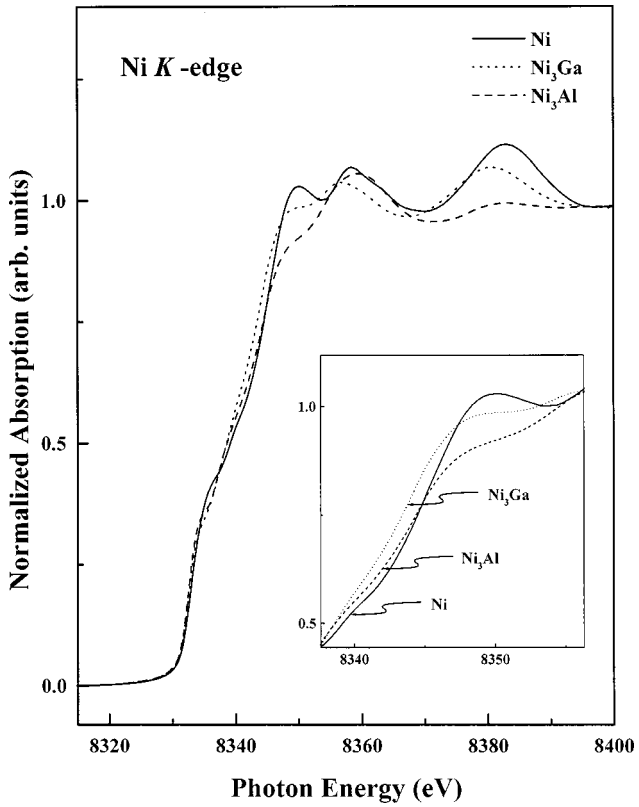


FIG. 3. Normalized Ni *K*-edge x-ray absorption spectra of the $Ni_3Al$ and $Ni_3Ga$ alloys and pure Ni at room temperature. The region of threshold edge in the inset is on a magnified scale.

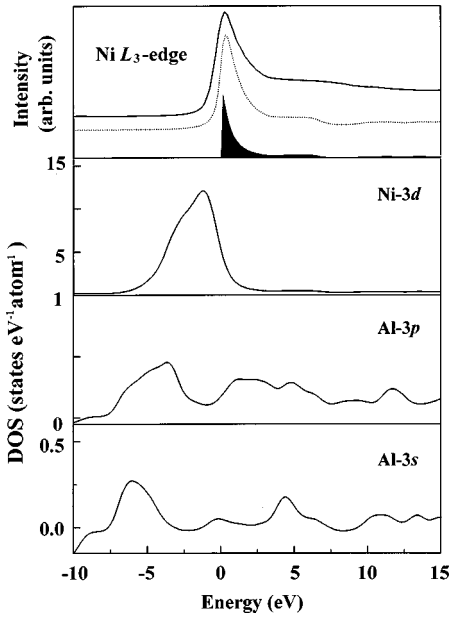


FIG. 4. Comparison of the Ni $L_3$-edge x-ray absorption near edge features (upper solid-line) with a convolution of the theoretical Ni *d*-projected DOS with core-hole lifetime and instrumental broadening (upper dashed-line) for $Ni_3Al$. The spectra have been aligned at the position of the first peak, and the intensity units have been normalized arbitrarily. The darkened area is the theoretical Ni *d*-projected DOS above the Fermi level, which is defined as the zero energy.

trostatic energy. Although electroneutrality is the general rule, charge redistribution of localized *d* electrons and itinerant *sp* type conduction electrons according to the relative electronegativity of the constituent metal atoms can still occur without any significant net charge flow on and off a site in alloys.[17–19] One would intuitively expect that the Ni levels should shift to the lower photon energy in $Ni_3Al$ opposite to the shift to the higher photon energy of the Al *p*-derived states. However, the Ni $3d$ states in $Ni_3Al$ and $Ni_3Ga$ do not shift noticeably towards the lower photon energy at the Ni $L_{3,2}$ edge as shown in Fig. 1. Thus, we argue that the charge transfer occurs not only through the Al $3p$(Ga $4p$)-Ni $3d$ hybridized states, but also through the rehybidized *s*-*p*-*d* states involving one or two sites in $Ni_3Al$ ($Ni_3Ga$). The involvement of conduction electrons of Ni $p$ character in rehybridization can be evidenced in the Ni *K*-edge XANES, which probes the unoccupied Ni $4p$-derived states above the Fermi level. Figure 3 displays the Ni *K*-edge XANES of $Ni_3Al$, $Ni_3Ga$, and pure Ni. According to this figure, the absorption intensity above the main edge decreases noticeably and the shift of their main edges towards the lower photon energy for both $Ni_3Al$ and $Ni_3Ga$ are comparable with that of pure Ni. The pre-edge shoulder in the Ni *K*-edge XANES can be attributed to the Ni $1s$ to $3d$ transition through the Ni $p$-$d$ rehybridization.[18] A reduction of the Ni *K* near edge intensity corresponds to the reduction of the number of unoccupied Ni $4p$-derived states, which implies an enhancement of the number of occupied Ni $4p$-derived states and a gain of Ni $4p$-orbital charge upon alloying. To maintain local charge neutrality, Ni must lose some *s*-orbital charges in both $Ni_3Al$ and $Ni_3Ga$ and the density of unoccupied Ni *s*-derived states in the vicinity of the Fermi level should increase in both $Ni_3Al$ and $Ni_3Ga$ relative to that of pure Ni. This indeed can be found in the satellite structure $B_1$ at the Ni $L_3$ edge of the XANES spectra for $Ni_3Al$ and $Ni_3Ga$ as shown in Fig. 1, which can be seen to be relatively dispersive and stronger. This observation is consistent with the difference curve of the Ni $L_3$-edge spectra between the alloys and pure Ni as shown in the inset of Fig. 1. The intensities of $\Delta A_1$ (between 850.0 and 856.6 eV) and $\Delta B_1$ (between 856.6 and 865.0 eV) were integrated separately for the $Ni_3Al$ and $Ni_3Ga$ spectra. The integration yielded $-0.62\pm0.03$ and $0.60\pm0.03$ for $Ni_3Al$ and $-0.38\pm0.02$ and $0.33\pm0.02$ for $Ni_3Ga$ for $\Delta A_1$ and $\Delta B_1$, respectively. These results indicate that the loss in $\Delta A_1$ (indicating that Ni $3d$ orbitals gain electron charge) is almost compensated by the gain of $\Delta B_1$ (indicating that Ni $4s$ orbital loses electron charge) in $Ni_3Al$ and $Ni_3Ga$.

Figures 4 and 5 compare Ni $L_3$-and Al *K*-edge XANES spectra with calculated Ni *d*-projected and Al *p*-projected DOS of $Ni_3Al$, respectively. The darkened area shows the theoretical Ni *d*-projected and Al *p*-projected DOS above the Fermi level. The upper solid curve is the Ni $L_3$- and Al *K*-edge absorption spectra at the region of XANES. The dashed curve in the middle represents the theoretical Ni *d*-projected (Al *p*-projected) DOS broadened with a Lorentzian of 0.3 eV (0.42 eV) to simulate the core-hole lifetime[20] and convoluted with a Gaussian function of 0.4 eV (0.5 eV) to simulate the experimental resolution. According to Figs. 4 and 5, the Ni $3d$ states lie predominantly below and near the Fermi level with a relatively small DOS above the threshold region in comparison with those of Ni $4sp$ and Al $3sp$ states.

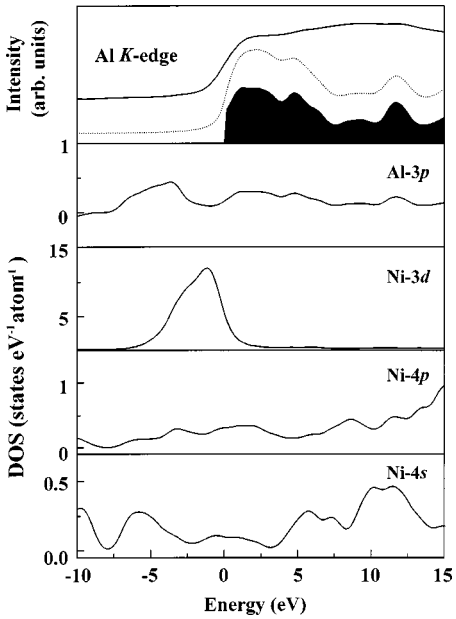


FIG. 5. Comparison of the Al *K*-edge x-ray absorption near edge features (upper solid-line) with a convolution of the theoretical Al *p*-projected DOS with core-hole lifetime and instrumental broadening (upper dashed-line) for $Ni_3Al$. The spectra have been aligned at the position of the first peak and the intensity units have been normalized arbitrarily. The darkened area is the theoretical Al *p*-projected DOS above the Fermi level, which is defined as the zero energy.

The DOSs for Ni $4sp$ and Al $3sp$ states spread over a wide energy range because they are more delocalized or extended. Our calculations also reveal that the white-line features $A_1$ and the satellite structure $B_1$ observed at Ni $L_3$-edge XANES in Fig. 1 is primarily contributed by Ni $3d$-derived states, which hybridize with the Al $3sp$ states. On the other hand, peaks $A_2$ and $B_2$ at the Al *K*-edge XANES of $Ni_3Al$ shown in Fig. 5 can be attributed to the Al $3p$-derived states, which hybridize with the Ni $3d/4sp$ states. In particular, the Al $3p$-Ni $3d/4sp$ hybridized states are found to contribute significantly to features $B_2$ at the Al *K*-edge XANES spectra of $Ni_3Al$. Similar results have also been obtained for the $Ni_3Ga$ alloy. These results agree with our experimental data and confirm the presence of strong Ni–X hybridized bonds in the Ni-based intermetallic $Ni_3X$ systems.[4–8]

Table II summarizes the calculated numbers of electrons ($e$) occupying the valence orbitals of Ni and Al in the alloy and pure Ni and Al. Although recent augmented plane wave (APW) calculations showed that there is no unique definition of charge at a particular atomic site and charge transfer between two sites and they were found to depend on the muffin-tin radii of Al and Ni,[21,22] we believe these problems are characteristics of the plane-wave based methods because these methods cannot unambiguously assign interstitial charge to any particular atom. In contrast, the PSF method used in this study has an atom-centered muffin-tin-orbital basis set. Charges and charge transfer can be unambiguously determined through the occupation numbers of muffin-tin orbitals. Table II shows that Ni $3d$ states in $Ni_3Al$ and $Ni_3Ga$ gain a significant amount of charge relative to that of pure Ni, which qualitatively explain the variation of white-line features $A_1$ between alloys and pure Ni at the Ni $L_3$ edge as shown in Fig. 1. Since the intensity of $A_1$ is proportional to the density of unoccupied Ni $3d$ states, these calculated results imply a decrease of $A_1$ intensities in $Ni_3Al$ and $Ni_3Ga$ relative to that of pure Ni. Results of Ni $d$ electron counts in $Ni_3Al$ and pure Ni shown in Table II are consistent with earlier calculations.[7] The slightly larger charge transfer from Al to Ni $d$ orbitals in $Ni_3Al(0.29e)$ than that from Ga to Ni $d$ orbitals in $Ni_3Ga(0.24e)$ agrees with the results of Ni $L_3$-edge measurements. These measurements reveal a slightly smaller intensity of Al in $Ni_3Al$ than in $Ni_3Ga$. The calculated number of Al $p$ electrons decreases slightly from pure Al (1.48e) to the alloy $Ni_3Al(1.46e)$, which corresponds to the results of Al *K*-edge XANES shown in Fig. 2. The calculated number of Al $s$ electrons decreases from pure $Al(1.51e)$ to the $Ni_3Al$ alloy $(1.20e)$. The calculated number of Ni $s$ electrons decreases slightly from pure $Ni(0.58e)$ to $Ni_3Al/Ni_3Ga(0.54e)$. The numbers of $s$ electrons transferred away from the Ni $4s$ orbital in the alloys are relatively small $(0.04e)$ comparing to that inferred from our experimental observations of a stronger $B_1$ features in $Ni_3Al$ and $Ni_3Ga$ than in pure Ni. These results agree with the earlier discussion that Ni $d$ orbitals in the alloys gain some electron charges with the expense of non-$d$ conduction electrons ($s$ electrons). The direction of charge transfer is in accordance with the higher electronegativity for Ni (1.91) than for Al (1.61) and Ga (1.81). If $\Delta n(\mathrm{Ni})[\Delta n(\mathrm{Al})]$ is the difference in the electron counts in the Ni (Al) orbitals between $Ni_3Al$ and pure Ni (Al), then $\Delta n(\mathrm{Ni}) = n_{\mathrm{spd}}(\mathrm{Ni_3Al}) - n_{\mathrm{spd}}(\mathrm{Ni})[\Delta n(\mathrm{Al}) = n_{\mathrm{sp}}(\mathrm{Ni_3Al}) - n_{\mathrm{sp}}(\mathrm{Al})]$. $\Delta n$'s can be obtained from the numbers of electrons occupying Ni and Al orbitals given in Table II. The charge transferred into the Ni orbitals is $+0.26e$, which roughly equals the charge transferred away from the Al orbitals $(-0.33e)$ in the $Ni_3Al$ alloy. This is consistent with the observation that the intensities of the white-line $A_1$ features are considerably reduced in $Ni_3Al$ and $Ni_3Ga$ as shown in Fig. 1, which implies a gain of Ni $3d$-orbital charge. The Ni $L_{3,2}$-edge XANES spectra do not have any noticeable shifts relative to that of pure Ni, suggesting some non-$d$ charge depletion at the Ni sites in the alloy. Moreover, the absorption intensity above the Ni *K*-edge XANES in $Ni_3Al$ and $Ni_3Ga$ decreases relative to that of pure Ni as shown in Fig. 3, which suggests that the Ni $p$ orbitals also gain electron charges upon alloying, further demonstrating that the depleted charge at the Ni site consists primarily of itinerant $s$ electrons. It seems that our calculated $s$-orbital occupation numbers disagree with the observed depletion of $s$ electrons at the Ni sites. But we would like to mention that in our calculations, $s$ orbitals,

TABLE II. Total integrated number of electrons per atom for the valence orbitals at the Ni and Al sites in $Ni_3Al$, $Ni_3Ga$, and reference pure Ni and Al.

| | Ni site | | | Al site | |
|---|---|---|---|---|---|
| | $n_s$ | $n_p$ | $n_d$ | $n_s$ | $n_p$ |
| Ni | 0.58(0.02) | 0.60(0.03) | 8.59(0.03) | | |
| $Ni_3Al$ | 0.54(0.04) | 0.61(0.03) | 8.88(0.03) | 1.20(0.02) | 1.46(0.02) |
| $Ni_3Ga$ | 0.54(0.02) | 0.60(0.03) | 8.83(0.02) | | |
| Al | | | | 1.51(0.01) | 1.48(0.01) |

which are different from *d* orbitals, are extended Bloch orbitals; they are not localized at the atomic sites. In our calculations the local charge neutrality is implicitly guaranteed by the itinerant nature of *sp* electrons through the screening effect, which is characteristic of metallic systems.

As generally believed, the *p-d* hybridization effect in transition-metal compounds is closely related to the energy separations between the transition-metal *d* and the nearest-neighbor (NN) *p* states as well as the transition-metal-NN bond lengths.[23] Harrison showed that the square of the hybridization coupling constant, $V_{pd}^2$, is proportional to $(r_d^3/d_{NN}^7)$,[24] where $r_d$ and $d_{NN}$ are the transition-metal *d*-orbital radius and the transition-metal-NN bond lengths, respectively. The strength of Al(Ga) *p*-Ni *d* hybridization in $Ni_3Al$ ($Ni_3Ga$), which is predominantly determined by the degree of overlap of the participating Ni *d* and Al(Ga) *p* orbitals, should be closely associated with the electronic transition probabilities occurring between Ni $3d$- and Al $3p$-(Ga $4p$-) derived states as well as the NN Ni–Al (Ga) bond lengths. To see if this is the case, we obtained the NN bond lengths of $2.54 \pm 0.01$ Å in $Ni_3Al$ (Ni–Al) and $2.59 \pm 0.01$ Å in $Ni_3Ga$ (Ni–Ga) using the extended x-ray absorption fine structure (EXAFS) at the Ni *K*-edge in $Ni_3Al$ and $Ni_3Ga$, respectively.[25] The NN bond lengths obtained by careful EXAFS analysis give rise to a slightly greater *d-p* coupling constant in $Ni_3Al$ than in $Ni_3Ga$. This difference is consistent with the greater size of the Ga atom (covalent radius $= 1.26$ Å) than the Al atom (covalent radius $= 1.18$ Å),[12] which leads to a slightly greater *p-d* hybridization in $Ni_3Al$ than in $Ni_3Ga$ as predicted by the Harrison's formula. This conclusion is consistent with earlier theoretical calculations, in which Iotova *et al.*[6] obtained slightly smaller *d-p* energy difference, i.e., $E_d(\mathrm{Ni}) - E_p(\mathrm{X})$, and a slightly larger *d-p* coupling constant for $Ni_3Al$ than for $Ni_3Ga$.

## V. CONCLUSION

The observed decrease in the intensity of white-line features at Ni $L_3$ edge and the edge energy shifts towards the lower photon energy at the Ni *K*-edge XANES relative to that of pure Ni imply an enhancement of Ni $3d$-states filling. The threshold at the Al *K*-edge XANES for $Ni_3Al$ shifts towards the higher photon energy relative to that of pure Al, which implies that Al loses some *p*-orbital charges in $Ni_3Al$. Thus, there is charge transfer from Al $3p$ to Ni $3d$ orbitals. We also found that Ni $p$ orbitals gain some electrons. The property of the local charge neutrality of this metallic system is maintained through the loss of itinerant *s* electrons at the Ni site to compensate the gain in Ni $4p$ and $3d$ electrons. A prominent feature $B_2$ observed in the $Ni_3Al$ spectrum at the Al *K* edge can be attributed to the Al $3p$-derived states, which hybridized strongly with Ni $3d/4sp$ states. Our EXAFS analysis showed that the NN Ni–Al bond length is shorter than that of Ni–Ga. The use of the Harrison's formula indicates that the Ni $3d$ states have a stronger hybridization with the Al $3p$ states in $Ni_3Al$ than with the Ga $4p$ states in $Ni_3Ga$.

## ACKNOWLEDGMENTS

One of the authors (W.F.P.) would like to thank the National Science Council of R.O.C. for financially supporting this research under Contract No. NSC 89-2112-M-032-008. SRRC is also appreciated for the use of their HSGM and wiggler beamlines to perform this study.

[1] N. S. Stoloff, Int. Met. Rev. **29**, 123 (1984).
[2] J. K. Okamoto, C. C. Ahn, and B. Fultz, J. Appl. Phys. **77**, 4380 (1995).
[3] D. A. Muller, S. Subramanian, P. E. Batson, S. L. Sass, and J. Silcox, Phys. Rev. Lett. **75**, 4744 (1995).
[4] Zs. Kovács, L. Kövér, P. Weightman, D. Varga, R. Sanjinés, J. Pálinkás, G. Margaritondo, and H. Adachi, Phys. Rev. B **54**, 8501 (1996).
[5] J. C. Fuggle, F. U. Hillebrecht, R. Zeller, Z. Zolnierek, P. A. Bennett, and Ch. Freiburg, Phys. Rev. B **27**, 2145 (1982).
[6] D. Iotova, N. Kioussis, and S. P. Lim, Phys. Rev. B **54**, 14413 (1996).
[7] D. Hackenbracht and J. Kübler, J. Phys. F **10**, 427 (1980).
[8] S. N. Sun, N. Kioussias, S. P. Lim, A. Gonis, and W. H. Gourdin, Phys. Rev. B **52**, 14421 (1995).
[9] L. S. Hsu, K. L. Tsang, and S. C. Chung, Mater. Res. Soc. Symp. Proc. **437**, 53 (1996).
[10] R. V. Kasowski, M.-H. Tsai, T. N. Rhodin, and D. D. Chambliss, Phys. Rev. B **34**, 2656 (1986); M.-H. Tsai and K. C. Hass, *ibid.* **51**, 14616 (1995); K. C. Hass, M.-H. Tsai, and R. V. Kasowski, *ibid.* **53**, 44 (1996).
[11] *International Tables for X-Ray Crystallography*, edited by N. F. M. Henrand and K. Lonsdal (Kynoch, Birmingham, 1969), Vol. 1.
[12] *Table of Periodic Properties of the Elements* (Sargent-Welch Scientific Company, Skokie, IL, 1980).
[13] D. J. Chadi and M. L. Cohen, Phys. Rev. B **8**, 5747 (1973).
[14] H. J. Monkhorst and J. D. Pack, Phys. Rev. B **13**, 5188 (1976).
[15] G. van der Laan, J. Zaanen, G. A. Sawatzky, R. Karnatak, and J. M. Esteva, Phys. Rev. B **33**, 4253 (1986); G. van der Laan, B. T. Thole, G. A. Sawatzky, and M. Verdaguer, *ibid.* **37**, 6587 (1988).
[16] E. Tamura, J. van Ek, M. Fröba, and J. Wong, Phys. Rev. Lett. **74**, 4899 (1995).
[17] M. Kuhn and T. K. Sham, Phys. Rev. B **49**, 1647 (1994); I. Coulthard and T. K. Sham, Phys. Rev. Lett. **77**, 4824 (1996).
[18] T. K. Sham, A. Hiraya, and M. Watanabe, Phys. Rev. B **55**, 7585 (1997).
[19] H. H. Hsieh, Y. K. Chang, W. F. Pong, J. Y. Pieh, P. K. Tseng, T. K. Sham, I. Coulthard, S. J. Naftel, J. F. Lee, S. C. Chung, and K. L. Tsang, Phys. Rev. B **57**, 15204 (1998).
[20] See Appendix B, *Unoccupied Electronic States*, edited by J. C. Fuggle and J. E. Inglesfield (Springer, Berlin, 1992).
[21] D. A. Muller, D. J. Singh, and J. Silcox, Phys. Rev. B **57**, 8181 (1998).
[22] D. A. Muller, P. E. Batson, and J. Silcox, Phys. Rev. B **58**, 11970 (1998).
[23] B. E. Larson, K. C. Hass, H. Ehrenreich, and A. E. Carlsson, Phys. Rev. B **37**, 4137 (1988).
[24] W. A. Harrison, *Electronic Structure and the Properties of Solids* (Freeman, San Francisco, 1980).
[25] W. F. Pong *et al.* (unpublished).